# The UNAM-MARine Aerosol Tank (UNAM-MARAT): An Evaluation of the Ice-Nucleating Abilities of seawater from the Gulf of Mexico and the Mexican Pacific

M. Fernanda Córdoba[1], Rachel Chang[2], Harry Alvarez-Ospina[3], Aramis Olivos-Ortiz[4] Graciela B. Raga[1], Daniel Rosas-Ramírez[5], Guadalupe Campos[6], Isabel Márquez[3], Telma Castro[1], and Luis A. Ladino[1,*]

[1]Instituto de Ciencias de la Atmósfera y Cambio Climático, Universidad Nacional Autónoma de México, Ciudad de México, C.P. 04510, México

[2]Department of Physics and Atmospheric Science, Dalhousie University, C.P. B3H 4R2, Canada

[3]Facultad de Ciencias, Universidad Nacional Autónoma de México, México City, México

[4]Centro Universitario de Investigaciones Oceanológicas, Universidad de Colima, C.P. 28860, México

[5]Departamento de Química de Biomacromoléculas, Instituto de Química, Universidad Nacional Autónoma de México, Av. Universidad 3000, Circuito Exterior S/N, Coyoacán, Ciudad Universitaria, Mexico City, 04510, México

[6]Laboratorio de Alimento Vivo, Procuraduría Estatal de Protección al Medio Ambiente-Aquarium del Puerto de Veracruz, Blvd. Manuel Ávila Camacho s/n, Col. Ricardo Flores Magón, C.P. 91900. Veracruz, Veracruz, México

*Corresponding author: luis.ladino@atmosfera.unam.mx

Keywords: Ice Nucleating Particles, Sea Spray, Mexican Pacific Ocean, Gulf of Mexico.

## Abstract

Although several studies have shown that sea spray aerosol (SSA) has the potential to act as ice nucleating particles (INP) impacting cloud formation, there is a lack of marine INP studies in tropical latitudes. This is partly due to the unavailability of local oceanographic cruises that perform aerosol-cloud interaction studies in the tropics, as well as the scarcity of appropriate aerosol and cloud microphysics instrumentation. The present study shows the development of the UNAM-MARine Aerosol Tank (UNAM-MARAT), a device that simulates wave breaking to generate SSA particles with the main purpose to characterize their physicochemical properties including their ice nucleating abilities. The UNAM-MARAT was characterized using Instant Ocean Sea Salt and its potential to study ambient sea waters was evaluated with sea seawater samples collected from the Port of Veracruz (PoV) in the Gulf of Mexico, the Bay of Acapulco (BoA), and the Bay of Santiago-

Manzanillo (BoSM) in the Mexican Pacific Ocean. The portable and automatic UNAM-MARAT is able to generate aerosol particle concentrations as high as 2000 $cm^{-3}$ covering a wide range of sizes, from 30 nm to 10 μm, similar to those found in the ambient marine boundary layer. The SSA generated from the three natural seawater samples was found to act as INP via immersion freezing, with INP concentrations as high as 130.7 $L^{-1}$. The particles generated from the BoA seawater samples were the most efficient INPs, reporting the highest ice active site density ($n_s$) values between -20 and -30°C. Our results also show the direct relationship between particle size and its composition. Larger particles (> 1 μm) were found to be enriched in sodium chloride. In contrast, the fraction of $Ca^{2+}$, $Mg^{2+}$, and $NO_3^-$ was found to increase with decreasing the particle size from 10 μm to 320 nm. This suggests important differences in the presence of dissolved organic material in the submicron particles related to the sampling zone and possibly with the behavior of the SSA.

## 1 Introduction

Sea-Spray Aerosol (SSA) is ubiquitous in oceanic regions and forms via bubble bursting by wave breaking (Lamarre and Melville, 1991). It has been shown that SSA has the potential to impact the Earth's radiative balance (Jacobson, 2001) and the hydrological cycle given its capability to act as cloud condensation nuclei (CCN, Albrecht, 1989) and ice nucleating particles (INP, Boucher et al., 2013; Vergara-Temprado et al., 2017; McCluskey et al., 2018).

Laboratory experiments with diverse setups, including atomizers, nebulizers, and tanks (in acrylic, PTFE or stainless steel), to simulate SSA generation via bubble bursting, have been essential in determining the physicochemical and biological properties of SSA (Fuentes et al., 2010; McCluskey et al., 2017; Christiansen et al., 2019; Wolf et al., 2020). Some of these setups used different mechanisms for bubble production such as diffusers, glass frits or systems like plunging-water jet or sheetlike (Cipriano & Blanchard, 1981; Fuentes et al., 2010; Prather et al., 2013; Stokes et al., 2013; Christiansen et al., 2019). Using a small tank to produce SSA, Cipriano & Blanchard (1981) determined that bubbles with diameter > 1 mm can produce aerosol particles < 5 μm in diameter, while bubbles < 1 mm generate aerosol particles > 20 μm. However, it is currently believed that submicron (< 1 μm) and supermicron (> 1 μm) aerosol particles can be generated by the film drop and jet drop mechanisms, respectively (Resch & Afeti, 1992; Lewis & Schwartz, 2004; Burrows et al., 2014). Recently, Wang et al. (2017) found that the jet drop mechanism can produce up to 43% of submicron SSA.

Results from field measurements and laboratory experiments indicate that SSA exhibits a trimodal particle size distribution (PSD) with peaks observed at 0.02 - 0.05 μm, 0.1 - 0.2 μm, and 2 - 3 μm (Quinn et al., 2015). Laboratory experiments using artificial seawater in a 30 L marine aerosol tank, Sellegri et al. (2006) demonstrated that the trimodal PSD of the SSA can vary with other environmental variables such as sea surface temperature (SST). The

authors found that if SST decreases the peaks of the PSD are displaced towards smaller diameters. The presence of surfactants (e.g., sodium dodecyl sulphate, SDS) can also influence the amplitude of the modal peaks as surfactants extend the bubble lifetime at the surface, and then bubbles can be broken by wind or subsequent waves (Sellegri et al., 2006). Additionally, Hartery et al. (2022) found that adding sodium dodecyl benzene sulfonate, (SDBS, a surfactant) to a NaCl solution in the Dalhousie Automated Wave Tank (DAWT) reduced particle size mode, particle concentration, and hygroscopicity, further highlighting the impact of surfactants on aerosol properties. Using a similar experimental setup to the one used by Sellegri et al. (2006), Fuentes et al. (2010) found that the SSA submicron size distribution, its hygroscopicity, and its ability to act as CCN are not significantly affected by the bubble bursting generation mechanism (i.e., porous bubblers and plunging- water jet systems). Nevertheless, Fuentes et al. (2010) reported that the best system for SSA generation when using natural sea water was the plunging-water jet, which improves the reproduction of organic enrichment and PSD.

Stokes et al. (2013) implemented a new system for SSA generation that includes an intermittent plunging sheet of water in a plexiglass 210 L tank, called the Marine Aerosol Reference Tank (MART). This mechanism simulates the gravitational impingement of a waterfall and the intermittence better reproduces wave breaking to create turbulence, the bubble plumes, and foam formation. The interaction of freshly emitted SSA with volatile organic compounds present in the marine atmosphere has been evaluated in the MART. Trueblood et al. (2019) discovered that by exposing supermicron SSA to hydroxyl radicals (OH), a fragmentation of the nitrogen-rich species (e.g., amino sugars or amino acids) is observed, and therefore, there is a reduction in the organic matter present in the SSA.

In addition to the above-mentioned laboratory tanks, a large-scale experimental setup such as the Wave Channel have provided insights into SSA generation under realistic marine conditions. A large tank (33 m x 0.5 m x 1 m) was designed in the Hydraulics Laboratory at the Scripps Institution of Oceanography (SIO) in San Diego – United States (Collins et al., 2014). SSA is generated through a hydraulic-paddle- created waves, sintered glass filters, and an intermittent plunging sheet of water (Collins et al., 2014). Simulation of ocean dynamics and biological activity in the wave channel allowed Prather et al. (2013) to conclude that SSA is composed mainly of four types of particles: sea salt (SS), sea salt with organic carbon (SS-OC), organic carbon (OC), and biological (Bio) particles, with its chemical composition strongly linked to particle size. The authors reported that supermicron particles were dominated by SS and Bio, while submicron particles by SS-OC and OC. Prather et al. (2013) also reported that Na, Cl, Mg, and K largely contribute to the SS particles and that between 30 and 40% (v/v) of the SS-OC particles, correspond to organic matter. Ca and Mg were found to be present in the OC particles, and they are known to be able to form complexes with natural organic ligands (Quinn et al., 2015). Organic matter can accumulate in the air-ocean interface, forming a gel-like layer with properties that differ from the

underlying waters. This layer, known as the sea surface microlayer (SML), has a typical thickness that varies between 1 and 1000 µm (Wurl et al., 2017). In an experiment similar to that carried out in the wave channel by Prather et al. (2013), Wang et al. (2015) determined that marine submicron particles are enriched in aliphatic organic material and that the soluble oxidized organic compounds are found in supermicron particles. Additionally, Wang et al. (2015) showed that differences in the SSA chemical composition could result from a variety of biological processes, including bacterial activity and phytoplankton primary production.

It is well known that SSA can act as an INP (Bigg, 1973; Schnell & Vali, 1975; Schnell, 1977; Rosinski et al., 1987; Rosinski et al., 1988; Wilson et al., 2015; McCluskey et al., 2018). Several studies have suggested that marine species of phytoplankton are able to nucleate ice such as the *Heterocapsa niei* (dinoflagellate) (Fall and Schnell, 1985) and *Thalassiosira pseudonana* (diatom, Knopf et al., 2011; Alpert et al., 2011; Wilson et al., 2015). Through controlled laboratory experiments in the MART, DeMott et al. (2016) demonstrated that the INP number concentrations from seawater collected close to SIO - Pacific Ocean off the California coast, are within the range reported by previous studies in different maritime regions (Bigg, 1973; Schnell, 1977; Rosinski et al., 1988). However, the INP concentrations were lower than the corresponding concentrations in the surface boundary layer over continental regions. DeMott et al. (2016) also noted that the INP concentrations at -26 and -30°C were a factor of 50 larger after nutrient addition than freshly collected seawater. Wang et al. (2015) found that maximum concentrations of INP at ≥ -15ºC coincided with the peaks of the phytoplankton bloom carried out in the wave channel. These experiments used seawater from the Pacific Ocean near the SIO, suggesting that the observed ability to act as INP could be due to amphiphilic long-chain alcohols monolayer and that the ice nucleating activity (INA) was reduced when the samples went through the heating test, a process to denature biological INP (Hill et al., 2016). McCluskey et al. (2017) used seawater collected from the Pacific Ocean at the end of Scripps Pier (32°49′58.12″ N, -117°16′16.58″ W) in the MART. Their study suggests that microorganisms and biomolecules contribute to the INP population due to an increase of organic compounds during high INP concentrations.

Studies on INPs along the Mexican coasts and oceans are scarce. A pioneering study by Rosinski et al. (1988) in the Gulf of Mexico (GoM) demonstrated that the efficiency of aerosol particles as INP varies depending on their size, season, and sampling location. The influence of environmental conditions on the ice nucleation efficiency of marine aerosol particles was also evidenced by Ladino et al. (2019) and Córdoba et al. (2021). Both studies found that the arrival of cold air masses to the Yucatan Peninsula (Mexico) from higher latitudes increased the INP concentrations with aerosol particles capable to nucleate ice at -3°C.The warm freezing temperature suggests the influence of biological material, likely linked to bacteria and fungi from terrestrial and/or marine sources. Although the analyzed samples were not airborne particles, Ladino et al. (2022) found that the sea subsurface water (SSW) samples from the GoM exhibited better ice nucleation abilities than the sea surface

microlayer (SML) samples, contrary to the findings of Wilson et al. (2015) at higher latitudes. This discrepancy could be attributed to a lower organic material content in the SML samples of the GoM compared to those analyzed by Wilson et al. (2015). This difference in nucleation efficiency was also associated with low phytoplankton concentrations during the sampling period in the GoM, a crucial variable in the efficiency of particles as INPs.

Investigating SSA's role in marine environments is imperative for improving the accuracy of climate predictions (Burrows et al., 2022). Given that SSA ability to act as INP varies spatially and temporally (Burrows et al., 2013; Wilson et al., 2015; DeMott et al., 2016) and the scarcity of ice nucleation studies in tropical latitudes over maritime regions (Rosinski et al., 1988; Yakobi-Hancock et al., 2014; Wolf et al., 2020; Córdoba et al., 2021; Ladino et al., 2022; Melchum et al., 2023), expanding research efforts to study unexplored regions, such as the Mexican coasts, is of high importance. By advancing our understanding of SSA dynamics, we can enhance the accuracy of atmospheric models and reduce the uncertainties associated with aerosol-cloud interactions, thereby, contributing to more robust climate projections. The present study involves the building and characterization of a new device to generate SSA by simulating wave breaking through the intermittent plunging sheet of water mechanism, similar to the Stokes et al. (2013) tank, utilizing water samples from seawater collected offshore the Mexican coasts.

## 2 Instrument development

### 2.1 Description and Operation of the UNAM-MARAT

The UNAM - MARine Aerosol Tank (UNAM-MARAT) was built based on the design of Stokes et al. (2013) to study the physicochemical properties of SSA and its ability to nucleate ice under controlled conditions in the laboratory, using samples obtained from the oceanic waters that surround Mexico.

The UNAM-MARAT consists of an acrylic tank of 42 cm (length) x 32 cm (width) x 60 cm (height) with a total volume of 80.6 L. The tank has a lid of the same material, and to close the tank, the lid is tightened with ten screws; ambient air leaks are prevented by a neoprene O-ring placed between the lid and the tank-body as shown in Figure 1. A waterfall is generated by commercial 30.5 cm long cascade (DYNASTY SpaParts.com), placed at the back of the tank. Other cascades were tested; however, the commercial cascade was selected as it generated the highest concentration of aerosol particles (Sect. 3.2). Given that the tank is typically filled with 40 L of water, the height of the waterfall is about 22.5 cm from the water. On one side of the tank, a ½" orifice is used as an air intake. Ambient air passes through a high-efficiency particulate filter (HEPA - TSI, # 16020551) for particulate matter $\geq 0.3$ µm and a black carbon filter (PALL, PN 12011) to retain volatile compounds before entering the tank. Aerosol particles generated in the tank are sampled from the top of the tank through a ¼" orifice. A 1.0" orifice at the bottom of the tank is part of the water circulation system.

The circulation system consists of 1.0" internal diameter hoses, PVC pipes, and fittings (Fig. 1), a drain valve at the bottom and an on-off valve. The water is pumped with a centrifugal pump (Little Giant PondWorks, model 2-MDQ-SC), and the intermittent automatic water flow is generated and controlled with a corrosion-resistant ½" PVC solenoid valve (WIC VALVE, model 2PCZ-1/2-D-L) and a programmable time-delay relay (Macromatic Relay, Model TR 65122). The water flow is continuously monitored with a flowmeter (GPI TM SERIES, model TM050-N).

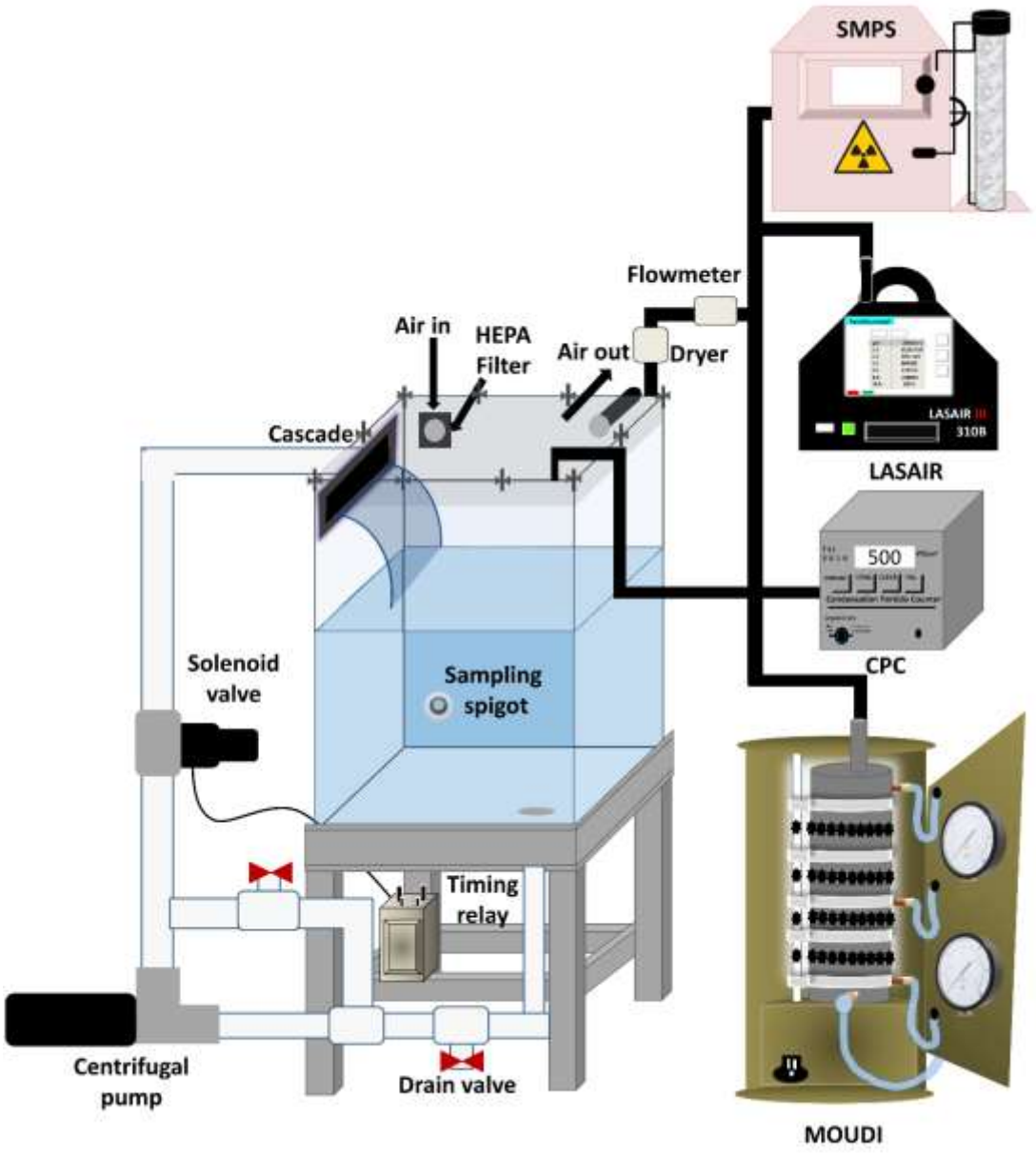


Figure 1. Diagram of the UNAM-MARAT experimental setup and the location of additional instrumentation.

Prior to each experiment, the tank is cleaned twice: first with distilled water and then with a mixture of isopropanol and distilled water. The distilled water and the 10% isopropanol solution are recirculated for 30 minutes. This procedure is carried out to eliminate residues and microorganisms from previous experiments. Once the system is cleaned, 10 L of the sample to be used are added to the tank and recirculated for 30 mins to purge it. Subsequently, the tank is completely emptied and filled with 40 L of the water sample to be analyzed. The tank is carefully closed and left to stand overnight. To monitor SSA generation, a condensation particle counter (CPC 3010, TSI) is connected at the inlet located at the top of the tank and data is collected for 20 mins to determine the baseline (background) concentration. Afterward, the waterfall is turned on for 20 minutes to generate aerosol particles, and samples are then taken for 10 minutes. The waterfall operates intermittently to mimic wave breaking (the operating time was 2s on and 10s off). The samples were collected after 20 minutes of aerosol generation given that this time was set as the point where SSA reached a steady state.

## 2.2 Additional instrumentation

Online and offline measurements were made to characterize the SSA generated in the UNAM-MARAT. Due to different flow rates of the online and offline instrumentation, not all instruments sampled simultaneously.

SSA PSD for particles larger than 0.3 µm were measured with an optical particle counter (LasAir III 310B, Particle Measuring Systems) with cut sizes of 0.3, 0.5, 1.0, 3.0, 5.0, and 10 µm. The data was recorded every 11s and the instrument was operated at a flow rate of 28.3 L $min^{-1}$.

SSA PSD for particles ranging between 10 and 400 nm was measured with a Scanning Mobility Particle Sizer (SMPS, TSI). The SMPS setup included an electrostatic classifier (model 3080, TSI), a scanning differential mobility analyzer (DMA, model 3081), and a water condensation particle counter (WCPC, model 3787). The sample flow rate was set at 0.6 L $min^{-1}$. Measurements were taken in 10 consecutive runs, each lasting 5 minutes, while the waterfall was in operation.

SSA particles were collected as a function of their aerodynamic diameter using a micro-orifice uniform deposit impactor (MOUDI 100R, MSP) at a flow rate of 29.9 L $min^{-1}$. The cut sizes of MOUDI are 0.18, 0.32, 0.56, 1.0, 1.8, 3.2, 5.6 and 10.0 µm (Mason et al., 2015). Aluminum substrates of 47 mm (TSI) were used for the subsequent chemical composition analysis, while hydrophobic glass coverslips of 22 mm x 22 mm (HR3-215, Hamptom Research) were used for the subsequent INP analysis. During a typical experiment, samples were collected four times for 10 mins each, on the same substrate. The substrates were stored in sealed petri dishes at 4°C until analyzed.

## 2.3 Chemical analysis

Particles collected on the aluminum substrates were analyzed by ion chromatography. The substrates were cut and placed inside polyurethane bottles with 10 mL deionized water, and then placed in an ultrasonic bath (model 3510, Branson) for 1 h at 47°C, allowing for the desorption and fragmentation of organic and inorganic particles. Subsequently, the bottles were placed on a mechanical orbital shaker (model 3005, GFL) for 6 h at 350 rpm. Samples were then filtered with acrodisc syringe filters of 25 mm diameter with a pore size of 0.2 µm (Pall Corporation). Finally, the filtrate was stored at -4°C (Chow and Watson, 1999). The identification and quantification of anions ($Cl^-$, $NO_3^-$, $Br^-$, $SO_4^{2-}$, $PO_4^{3-}$) and cations ($Na^+$, $Mg^{2+}$, $Ca^{2+}$, $NH_4^+$, $K^+$) was performed by a Dionex model ICS-1500 chromatograph equipped with an electrical conductivity detector. A Thermo Scientific Dionex IonPac AS23-4 µm Analytical Column (4 mm x 250 mm) with Thermo Scientific Dionex CES 300 Capillary Electrolytic Suppressor module and the mobile phase was 4.5 mM $Na_2CO_3$ - 0.8 mM NaHCO at 1 mL $min^{-1}$ flow rate for anions and a Thermo Scientific Dionex IonPac CS 12A Cation-Exchange Column (4 mm x 250 mm) with the Thermo Scientific Dionex CES 300 Capillary Electrolytic Suppressor and the mobile phase was a solution of $CH_4SO_3$ 20 mM and 1 mL $min^{-1}$ flow rate for cations as described in Ladino et al. (2019).

The ice nucleation abilities, via immersion freezing, of the SSA particles were measured through the droplet freezing technique (DFT). Detailed information on the operation of the UNAM-DFT can be found in Córdoba et al. (2021); therefore, only a brief description is provided below. The UNAM-DFT consists of four modules: (i) a cold stage, (ii) a humid/dry air system, (iii) an optical microscope with a video recording system, and (iv) a data acquisition system. Each glass coverslip with the SSA is placed on the cold stage and isolated from the ambient atmosphere. Humid air is circulated through the system, inducing liquid droplet formation by water vapor condensation. When droplets reach a diameter of 170 µm (on average), dry air is injected to induce evaporation and to increase the distance between droplets and, hence, to avoid contact droplet freezing. The humid/dry air system and the valves of the cold stage are then closed, and the temperature of the sample holder is decreased from 0 to -40 °C at a cooling rate of 10 °C $min^{-1}$. Droplet freezing is detected when the droplet changes from bright to opaque as seen during the video analysis. Thus, the freezing temperature is determined through the data acquisition system.

The ice-active surface site density ($n_s$) was derived from Eq. (1) at -15, -20, -25, and -30°C following Si et al. (2018):

$$n_s(T) = \frac{[INP(T)]}{S_{tot}} \quad (1)$$

where [*INP(T)*] is the INP concentration ($L^{-1}$) at temperature (T) and $S_{tot}$ is the total surface area of all aerosol particles. Full details of the $n_s$ calculation can be found in the Supporting Information.

The [*INP(T)*] is obtained from Eq. (2) in Mason et al. (2015):

$$[INP(T)] = -ln\left(\frac{N_u(T)}{N_o}\right).\left(\frac{A_{deposit}}{A_{DFT}V}\right).N_o.f_{ne}.f_{nu,0.25-0.10\,mm}.f_{nu,1\,mm} \quad (2)$$

where $N_u(T)$ is the number of unfrozen droplets at a temperature $T(°C)$, $N_o$ is the total number of droplets (dimensionless), $A_{deposit}$ is the total area of the aerosol particles deposited on the MOUDI hydrophobic glass coverslip ($cm^2$), $A_{DFT}$ is the area of the sample analyzed by the DFT ($cm^2$), $V$ is the volume of air through the MOUDI (L), $f_{ne}$ is a correction factor to account for the uncertainty associated with the number of nucleation events in each experiment (dimensionless), and $f_{nu}$ is a correction factor to account for changes in particle concentration across each MOUDI sample (dimensionless).

## 2.4 Collection of ocean water samples

The seawater samples to generate the SSA with the UNAM-MARAT were collected at three different Mexican coastal sites (Figure 2): The Port of Veracruz (PoV, Veracruz), the Bay of Acapulco (BoA, Guerrero), and the Bay of Santiago-Manzanillo (BoSM, Colima). The coordinates are given in Table S1. Approximately 60 L of seawater were collected in 20 L polyethylene containers previously washed with distilled water and purged with seawater. The samples were transported to Mexico City at room temperature. In the case of the BoSM samples, the UNAM-MARAT was deployed to the Water Quality Laboratory located in the University Center for Oceanological Research, University of Colima, Manzanillo, where some experiments were carried out in-situ. A second 60 L of seawater from the BoSM sample was collected (04/09/2022) and transported to Mexico City to evaluate potential changes that may occur during transportation. The sample was transported and stored at room temperature. Before introducing the seawater into the UNAM-MARAT, the samples were filtered with a 50 µm mesh to remove some debris and zooplankton.

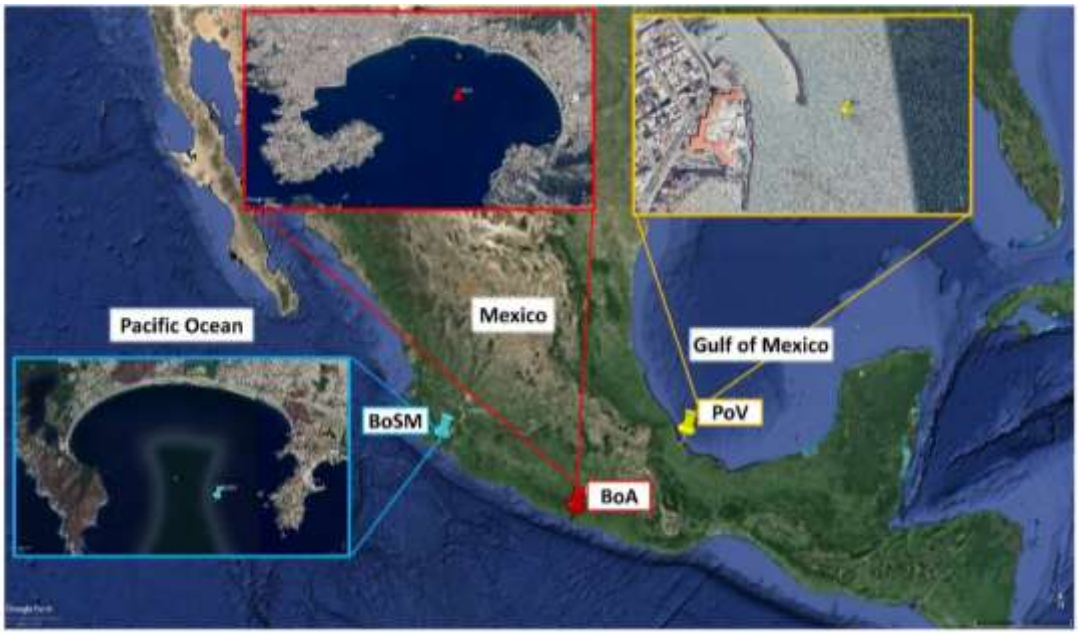


Figure 2. Map showing the sampling locations: The Bay of Acapulco (BoA, red icon), the Port of Veracruz (PoV, yellow icon), and the Bay of Santiago-Manzanillo (BoSM, blue icon). Photo from Google Earth.

## 3 UNAM-MARAT validation

### *3.1 Background particle concentrations*

Air entering the UNAM-MARAT was filtered to ensure that the measured aerosol particles corresponded solely to those generated by seawater and not due to leaks in the tank. Note that filtered air passing through the CPC resulted in an aerosol concentration of less than 0.1 $cm^{-3}$.

Background experiments measured total particle concentrations with the CPC when the tank was filled only with commercial distilled water. An individual experiment consists in measuring the particle concentration for 20 min. This procedure was repeated over three consecutive days, both in the morning and the afternoon (local time). In total, 15 runs were conducted, and the results were averaged with their corresponding standard deviation. Figure 3 shows the average particle concentration from the tank when it was filled with distilled water with the commercial cascade off (black line) and with the commercial cascade on (blue line). The shaded areas represent the standard deviation of each curve. The average particle concentration oscillated between 7.8 and 13.2 ± 2.3 $cm^{-3}$ with the cascade off (the top left figure shows a zoom of the base line), which indicates that there is a low number of particles within the tank. These results are in accordance with those reported by Prather et al. (2013), who found a baseline < 20 $cm^{-3}$ in the Wave Channel. When the cascade was in operation,

aerosol particles were generated from the distilled water (up to 313 $cm^{-3}$), indicating that the water used was not completely free of particles. Also, given that the samples were not passed through a diffusion dryer, it is likely that the measured particles correspond to large water droplets that did not evaporate before entering the CPC.

A commercial sea salt (i.e., *Instant Ocean Sea Salt, IOSS*) was used as a proxy for sea water for the validation of UNAM-MARAT. For a typical experiment a solution was prepared in distilled water, achieving a salinity of 28.8 ± 0.2 g $L^{-1}$. The tank was filled with 40 L of an IOSS's solution and the total particle concentration was measured with the CPC. The average particle concentration is represented by the red line in Figure 3. It shows that the maximum concentration observed after 20 min of turning on the cascade was 1016 $cm^{-3}$. Figure 3 demonstrates that the UNAM-MARAT is capable of generating SSA, as indicated by the observed increasing concentration.

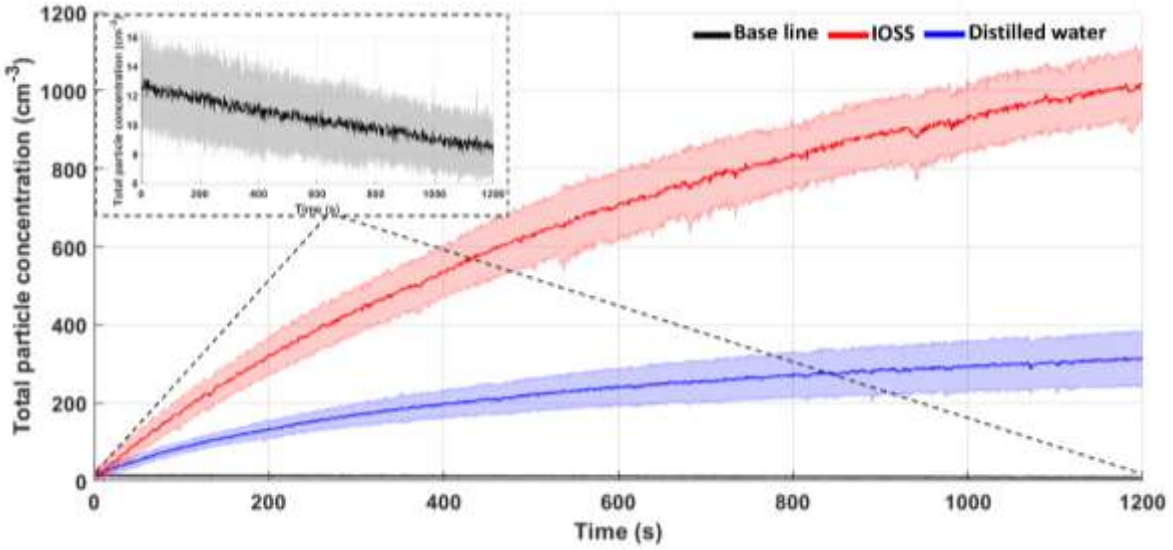


Figure 3. Total aerosol concentration as a function of the time (s) with the cascade off (black line in the inset in the upper panel), with the cascade on with distilled water (blue line) and with an IOSS's solution (red line). The shaded areas represent the standard deviation of each curve.

### *3.2 Cascade test*

To evaluate the role that the cascade plays in SSA generation in the UNAM-MARAT, the tank was filled with 40 L of an IOSS's solution and the total particle concentration was measured when using four different cascades: one was a commercial cascade and the other three were homemade. The homemade waterfalls consisted of cylindrical PVC pipes featuring a slot designed to facilitate the formation of a plunging water sheet. An internal tube with multiple evenly spaced holes was incorporated to enhance water distribution as shown in Figure S1. The main characteristics of each cascade produced with varying slot lengths, inner tube diameters and number of holes, are shown in Table S3.

The cascade A produced the lowest particle number concentrations, whereas the highest concentrations were observed with cascades C and D (Fig. 4). As shown in Table S3, the slot length of cascade D is longer than the other cascades, suggesting that the slot's length is a key factor in increasing particle generation. Cascade D (the commercial one) was selected for the subsequent experiments because it produced the highest particle concentration, its standard deviation was slightly lower than cascade C and it was the easiest to clean.

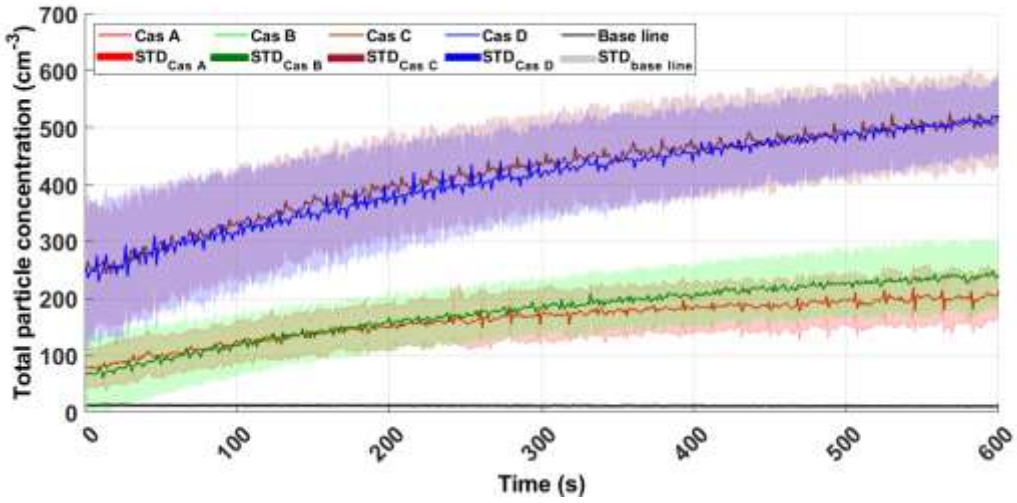


Figure 4. Total aerosol number concentration as a function of the time (s) for the different cascades. Each curve represents the average of fourteen experiments, with the shaded area representing the corresponding standard deviation.

In contrast, experimental results suggest that the number of holes in the inner cascade tube, and its diameter, play a secondary role in particle production. A longer slot length results in a larger artificially generated wave, through the plunging sheet of water mechanism rather than the plunging jet mechanism.

Stokes et al. (2013) noted that the shape and penetration of water drops (i.e., plunging sheet or plunging jet) affect aerosol particle production, with plunging sheet generating more particles. In contrast, other aerosol generation systems used in marine tanks have shown limited efficiency, as they often produce particles within a narrow size range. For instance, Fuentes et al. (2010) observed that systems employing glass frits and aquarium diffusers can produce high concentrations of particles, but these particle size typically range between 0.012 and 0.018 µm. This limitation arises because these systems primarily simulate the film drop mechanism. Plunging sheet systems, such as in the UNAM-MARAT, can produce a broader range of particles sizes, as they facilitate both the film and jet drop mechanisms, leading to more diverse aerosol size distributions (Stokes et al., 2013)

### *3.3 The intermittency time*

Waves in marine environments are not generated continuously, mainly due to the different energy processes that drive them, their intensity, and physical and physiographic aspects, resulting in an intermittent behavior (Jelley, 1989). Wang et al. (2017) revealed that a continuous cascade complicates the rupture of bubbles on the water surface, similarly affecting the formation of aerosol particles through the jet drops mechanisms, which is important in generating supermicron particles. For this reason, the solenoid valve controls the intermittence of the cascade and the operating time is modulated with a time-delay relay. Five intermittency values were evaluated: 2 s on / 10 s off, 4 s on / 10 s off, 2 s on / 4 s off, 2 s on / 6 s off, and 2 s on / 8 s off. The highest particle concentrations were observed for the 2 s on / 4 s off (~2400 $cm^{-3}$, Figure 5c) and 2 s on / 6 s off (~2000 $cm^{-3}$, Figure 5d) configurations, followed by the 2 s on / 8 s off (~1600 $cm^{-3}$, Figure 5e). For the 2 s on / 10 s off (Figure 5a), 4 s on / 10 s off (Figure 5b) configurations, the maximum aerosol concentrations were very similar (about 1400 $cm^{-3}$ after 600 s). Harb and Foroutan, (2019) also evaluated the role of the intermittency (i.e., 3 s on and 1s off, 3 s on and 2 s off, 3 s on and 3 s off, 3 s on and 4 s off, and 3 s on and 5 s off). The authors conclude that using a longer pause time to allow the bubble plume to develop, is beneficial for facilitating the mechanisms of film and jet drops production. However, it is important to note that the longer delay also allows for reformation of the SML, which is important in the composition of the marine aerosol. Although the 2 s on / 10 s off configuration did not report the highest particle concentration in the UNAM-MARAT, in the remainder experiments we choose this configuration to be comparable to the configuration used in Stokes et al. (2013). Additionally, using configurations 2 s on / 4 s off and 2 s on / 6 s off tend to create a more continuous plunging sheet, which could affect the size of the aerosol particles produced and may not accurately simulate the natural wave breaking processes.

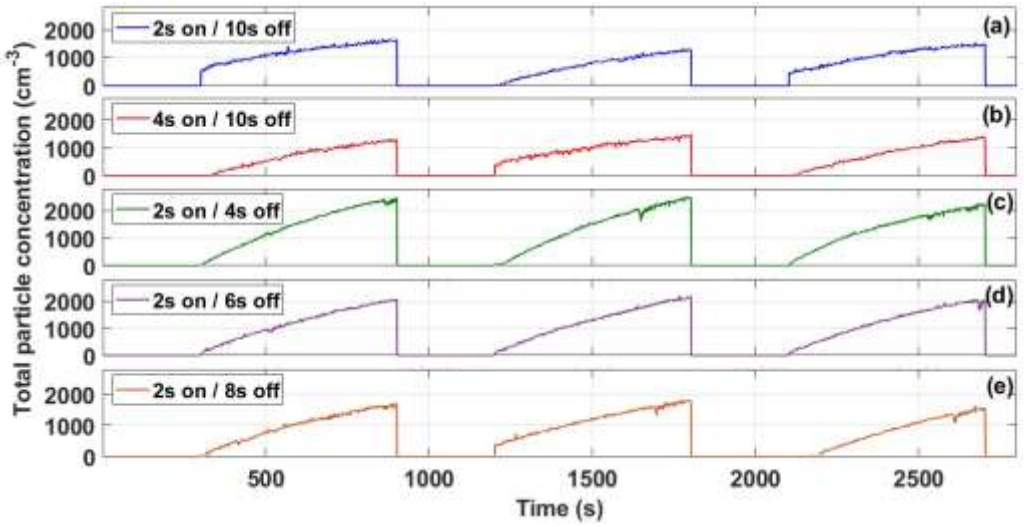


Figure 5. Total aerosol number concentration as a function of the time (s). The time series represent experiments with different intermittence values evaluated from an IOSS's solution in the UNAM-

MARAT. The different panels correspond to (a) 2 s on 10 s off, (b) 4 s on 10 s off, (c) 2 s on 4 s off (d), 2 s on 6 s off, and (e) 2 s on 8 s off.

Bates et al. (1998) reported that SSA concentrations measured in natural marine environments, such as the Southern Ocean were < 500 $cm^{-3}$. Concentrations achieved with the Wave Channel vary between 50 and 100 particles $cm^{-3}$, while experiments using artificial seawater (i.e., a salt mixture) conducted with the MART have reported particle concentrations ranging from 680 to 1053 $cm^{-3}$ (Thornton et al., 2023). The differences in the concentrations of particles generated in the MART, the Wave Channel, and the UNAM-MARAT tanks can be attributed to several factors, including the aerosol generation mechanism, the composition of the used seawater, and the specific design of each tank. For instance, the Wave Channel uses a paddle to create a disturbance for a wave generation, which affects aerosol production. In contrast, although the MART and the UNAM-MARAT employ similar mechanisms for aerosol generation, the particle concentration differences may be due to the different tank sizes: 210 L (MART) versus 80 L (UNAM-MARAT).

### *3.4 Waterfall height*

The importance of the waterfall height was assessed by testing different volumes of an IOSS's solution (salinity 28.8 ± 0.2 ppt). The total aerosol number concentration was measured for the following water volumes: 20, 30, 40, and 50 L which resulted in a waterfall height of 38.5, 30.5, 22.5, and 14.5 cm, respectively. Figure 6a shows the average total particle concentration (blue line) with their corresponding uncertainty (shaded area). The experiments for each water volume were performed over three different days.

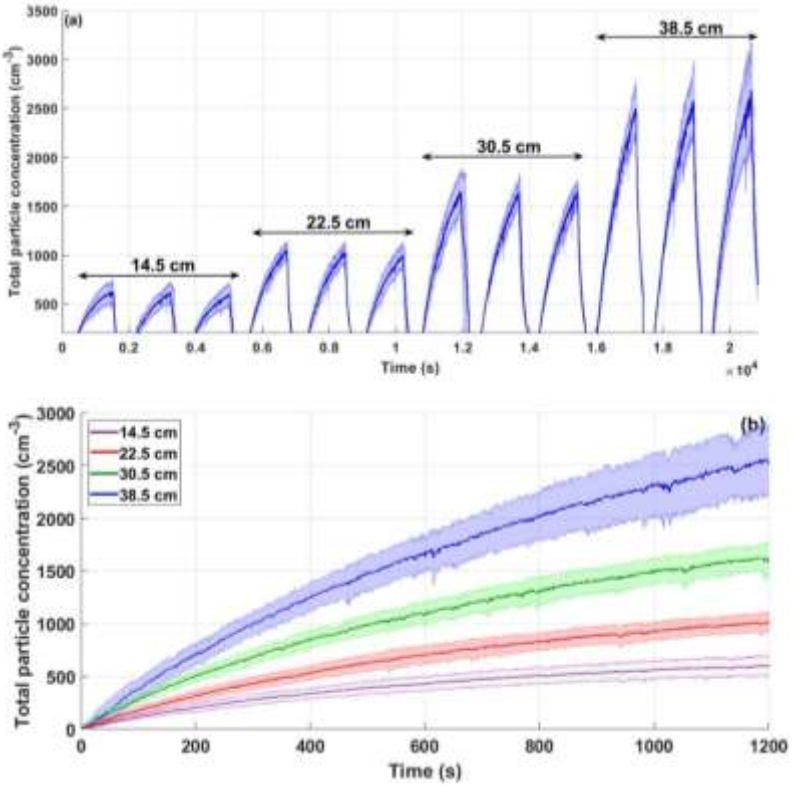


Figure 6. Total aerosol concentration as a function of the time (s). (a) the blue line shows the average of three days of repetitions from an IOSS's solution in the UNAM-MARAT. The shaded area represents the uncertainty of those repetitions. (b) Comparison of the average aerosol particle concentrations generated from different volumes with their corresponding uncertainty.

The highest concentrations were observed for the largest waterfall height (38.5 cm, 20 L of water), with concentrations up to 2500 $cm^{-3}$, followed by the waterfall height 30.5 cm (30 L of water), which reported a maximum concentration of 1600 $cm^{-3}$. The lowest concentration (600 $cm^{-3}$) were recorded for the waterfall height 14.5 cm (50 L of water). Notably, the uncertainty was low at the beginning of the experiments but increased over time (Figure 6b). Although the concentrations for the waterfall height 22.5 cm (40 L of water) were not as high as those reported for the waterfall height 38.5 cm, the uncertainty remained lower throughout the aerosol particle emission process. Therefore, this height was selected for most of the following experiments.

### *3.5 Particle size distribution*

The final step in characterizing the UNAM-MARAT was to evaluate the PSD of the generated SSA. The particle monitoring was conducted using a SMPS and a LasAir, to assess if the UNAM-MARAT could generate particles across a wide size range. The tank was filled with 40 L of an IOSS's solution and ten experiments were carried out using the intermittent cascade (2 s on, 10 s off). Figure 7a shows the PSD obtained with the SMPS for particles ranging between 10 nm and 400 nm. The black line represents the average of the ten

experiments, and the area between the blue lines indicates the standard deviation. A peak in concentration for particles between 0.1 and 0.2 µm in diameter was observed, corresponding to the accumulation mode. This mode is consistent with data reported using the MART (Stokes et al., 2013). Additionally, it is important to highlight that the UNAM-MARAT can produce coarse-mode particles (> 1 µm). The PSD obtained with the LasAir for particles ranging between 300 nm and 10 µm is presented in Figure 7b. The highest concentration was observed in the size bin corresponding to the smallest particles (i.e., 0.3 – 0.5 µm). These results demonstrate that the UNAM-MARAT can generate marine aerosol particles with sizes ranging from 30 nm to 10 µm.

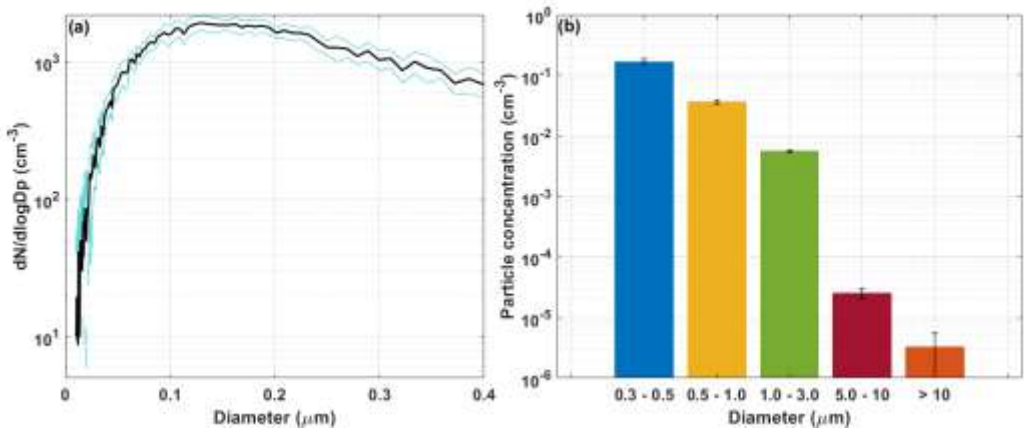


Figure 7. Aerosol particle size distribution obtained with the IOSS solution using (a) the SMPS and (b) the LasAir.

## 4 Case Study: Ice nucleating abilities of SSA

### *4.1 Aerosol particle concentrations and PSD*

This section presents the results obtained after generating SSA in the UNAM-MARAT using water samples from BoA, PoV, and BoSM. The results from BoSM correspond to samples collected on April 9, 2022, which were transported to Mexico City, as was the case with the BoA and PoV samples. The SSA generation experiments were performed on April 25, 2022. The highest number of particles generated with the UNAM-MARAT were obtained from the BoSM samples, showing concentrations up to 2000 $cm^{-3}$. In contrast, the lowest concentrations were observed from the PoV samples (570 and 590 $cm^{-3}$). This variation related to the origin of the samples may be due to differences in composition (inorganic and organic matter), as the equipment used to generate the SSA was the same and the protocol followed was identical. It is worth noting that at the time of collecting the BoSM samples, the water appeared very turbid. This could be attributed to a combination of organic matter

decomposition and suspended inorganic particulate matter. In comparison, the BoA and PoV samples had a clearer appearance.

Several factors, including nutrient availability, temperature, oxygen levels, light, and predation, determine the survival of microorganisms. The applied filtration may have removed grazers and other zooplanktonic organism, which could have influenced the development of microbial communities and, consequently, affected the aerosol concentrations. However, some studies suggest that certain species can withstand adverse conditions e.g., metabolic activity can slow down at lower temperatures or certain phytoplankton and bacteria species may persist in the absence of many predators (Chakraborty et al., 2012; Kennedy et al., 2019). Although it was not the scope of the present study, it is important to monitor how the evolution or degradation of biological species present in the seawater samples impact aerosol properties.

Mayer et al. (2020) reported particle concentrations ranging from 400 to 500 $cm^{-3}$ in an experiment with seawater collected at Scripps Pier, to which nutrients were added to promote phytoplankton blooms. Thornton et al. (2023) emphasize the importance of seawater composition in particle concentration. The authors conducted experiments in the MART, creating mesocosms with the *Thalassiosira weissflogii* diatom and the *Synechococcus elongatus* cyanobacterium, observing particle concentrations ranging from $1 \times 10^6$ to $2 \times 10^6$ $cm^{-3}$ for both species, with peaks reaching up to $6 \times 10^6$ $cm^{-3}$.

The PSD (for particles larger than 300 nm) from the different samples were comparable as shown in Figure 8. The highest concentrations were observed for particles in the smallest size bin i.e., 0.3 and 0.5 µm. Out of the three samples, the highest concentrations were observed in the BoSM samples for particles with diameters between 0.5 and 10 µm and in the PoV samples for particles between 0.3 and 0.5 µm. The numbers at the top of the bars in Figure 8 correspond to the average concentrations. Generally, the coarse particles correspond to sea salt (NaCl) and biological particles (intact or fragmented cells of bacteria, phytoplankton, macrogels, and transparent exopolymer particles, TEP) (Prather et al., 2013; Verdugo et al., 2004). Given that the most efficient INPs are likely particles > 500 nm (DeMott et al. 2010), the PSD for the ambient samples was only monitored using the LasAir (particles > 300 nm).

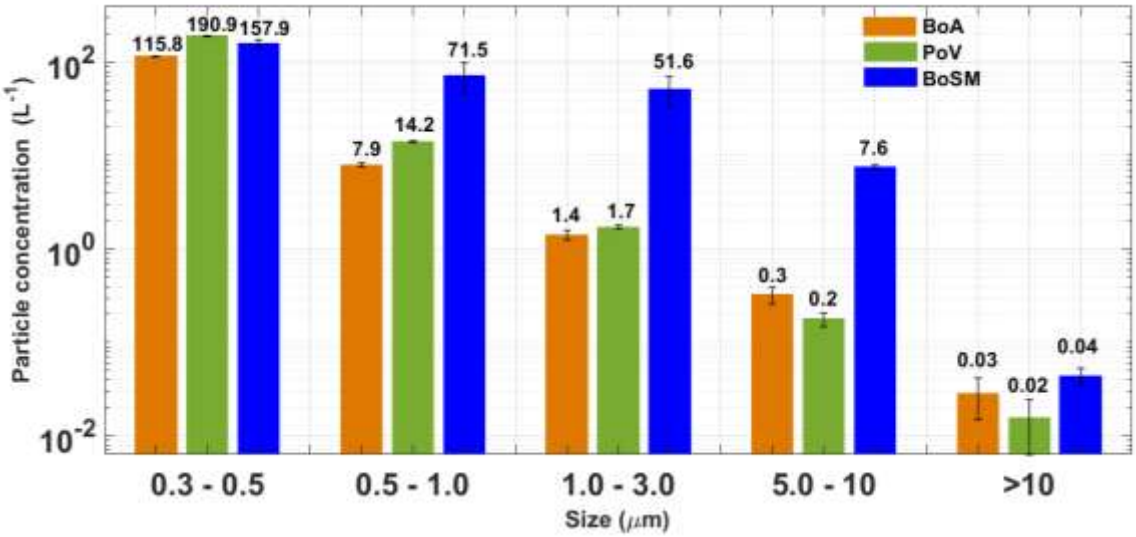


Figure 8. Aerosol particle size distribution for BoA (orange bars), PoV (green bars), and BoSM (blue bars). The error bars represent the standard deviation for each size bin.

### *4.2 Chemical composition*

To understand the differences in the chemical composition between samples, the concentration of ions as a function of particle size was analyzed for the PoV and BoSM samples (Figure 9). The BoA sample could not be processed for this specific analysis due to unintentional technical issues. As expected, the dominant ions were $Na^+$ and $Cl^-$ in both samples. Their concentration was highest for the largest particles (5.6 to 10 μm) and it was lowest for the smallest sizes (0.32- 0.56 μm). An opposite trend was observed for $Ca^{2+}$ and $Mg^{2+}$, as their concentration decreases with the particle size. Generally, $Ca^{2+}$ and $Mg^{2+}$ can interact with organic compounds such as carbohydrates, proteins, and lipids. Chin et al. (1998) demonstrated that a proportion of exopolymers present in seawater can assemble into gels through the chelation of $Ca^{2+}$ and $Mg^{2+}$, which form bridges between adjacent or different dissolved organic carbon (DOC) chains.

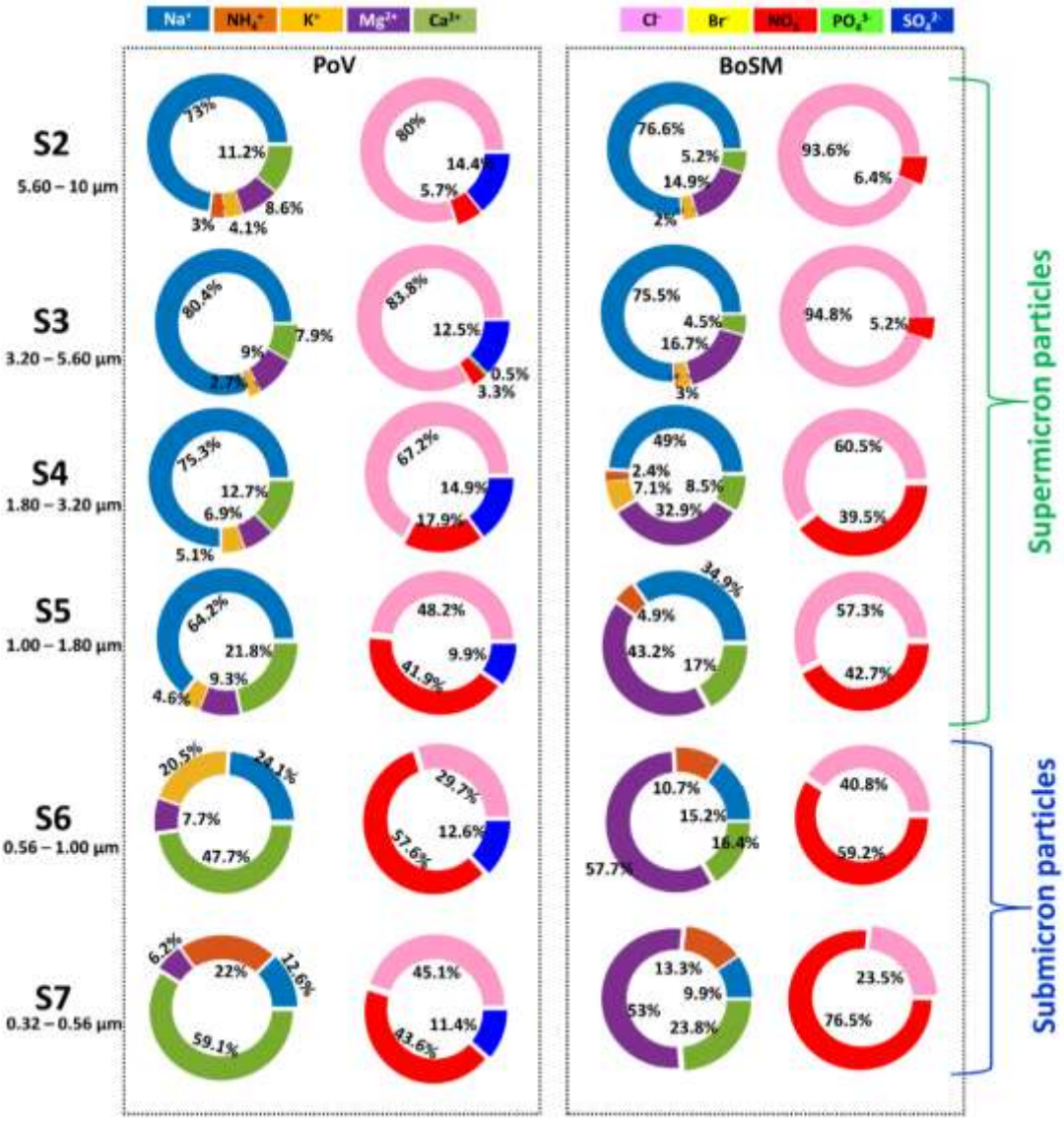


Figure 9. Ion concentration (mg $L^{-1}$) for each MOUDI stage for water samples collected in PoV (left panel), and BoSM (right panel). The pie charts on the left of each group represent cations, while those on the right represent anions.

Regarding the other ions, $NO_3^-$ showed a similar behavior as $Ca^{2+}$ and $Mg^{2+}$, while $NH_4^+$ increases with size from stage 4 (particle size: 1.80 - 3.20 µm) to stage 7 (particle size: 0.32 – 0.56 µm) for the BoSM sample. The presence of ions such as $NO_3^-$ and $NH_4^+$ may be due to the decomposition of organic matter or excretions of phytoplankton and zooplankton as well as the availability of nutrients in the environment from terrigenous origin by runoff, continental wind input or oceanographic process like a coastal upwelling (Anderson et al., 2002). The presence of $SiO_4^{-2}$ in the PoV sample may be the result of the dissolution of minerals rich in silicates of continental origin or of the dissolution of ortho silicic acid

($H_4SiO_4$) that is used in the biogeochemical cycle that is also regulated by phyto and zooplankton organisms (Kuuppo et al., 1998; Wu and Chou, 2003).

Bigg and Leck (2008) showed that particles with diameters smaller than 200 nm were exopolymers produced by bacteria and algae, as well as microgels formed from these exopolymers in laboratory experiments. Furthermore, the chemical composition of these particles is closely linked to biological activity. For instance, Facchini et al. (2008) demonstrated that submicron particles collected in the eastern North Atlantic off the coast of Ireland were predominantly composed of organic constituents. Russell et al. (2010) found that the majority of the organic components in submicron aerosol particles collected in the Arctic consisted of organic hydroxyl groups (including polyols and alcohols) characteristic of saccharides. Similarly, Bates et al. (2012) suggested that the organic mass from aerosol particles collected off the coast of California was composed of carbohydrate-like compounds containing organic hydroxyl groups, alkanes, and amines. Our results demonstrate that supermicron particles are largely dominated by sodium chloride. Additionally, our findings indirectly suggest that submicron particles also contain significant amounts of organic material, consistent with the findings reported by Prather et al. (2013).

### *4.3 INPs*

Figure 10a shows the concentration of INPs for the three set of samples as a function of temperature. The temperatures at which the different samples were able to nucleate ice, via immersion freezing, were found to be -19 to -34°C, -18 to -34°C, and -18 to -33°C for the BoA, PoV, and BoSM samples, respectively. The measured INP concentration ranged from 0.9 to 95.4 $L^{-1}$ for BoA, 1.7 to 97.5 $L^{-1}$ for PoV, and 0.9 to 130.7 $L^{-1}$ for BoSM. From these results, it can be inferred that there are no significant differences in the INPs concentrations among the water samples collected from the three sites.

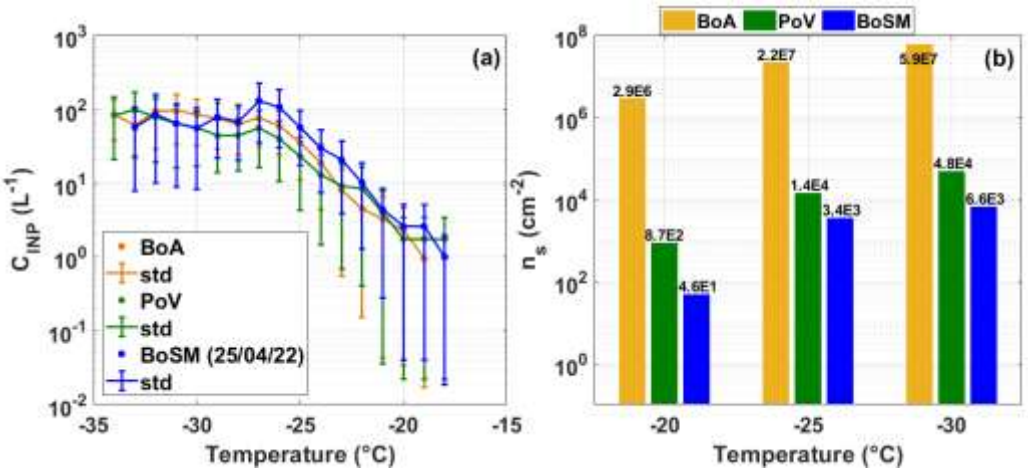


Figure 10. Comparison of the ice nucleating abilities between samples. (a) INP concentration as a function of temperature and (b) $n_s$ values as a function of temperature. Yellow, green and blue correspond to the BoA, PoV, and BoSM samples, respectively.

In an experiment conducted using the MART with seawater collected near SIO, DeMott et al. (2016) found that the INP concentrations varied between 1 x $10^{-3}$ and 1 x $10^{3}$ $L^{-1}$, with ice nucleation temperatures ranging from -7 to -30°C. The results observed in the marine aerosol samples generated with the UNAM-MARAT (this study) fall within the range reported by DeMott et al. (2016). Additionally, the findings in this study are consistent with those reported by McCluskey et al. (2017), who found that particles generated in the MART with waters collected near SIO, stimulated to produce phytoplankton blooms, were able to nucleate ice between -7 and -32°C, with INP concentrations ranging from 1 x $10^{-3}$ and 1 x $10^{1}$ $L^{-1}$. On the other hand, Thornton et al. (2023) reported that aerosol particles generated using the MART from waters containing *Thalassiosira weissflogii* and *Synechococcus elongatus*, as previously mentioned, exhibited ice freezing temperatures between -14 and -32°C. DeMott et al. (2016) and Thornton et al. (2023) concluded that the warmer freezing temperatures observed in their experiments coincided with peaks in chlorophyll a (Chl-a) in their mesocosms. In contrast, McCluskey et al. (2017) demonstrated that increases in INPs active between -25 and -15°C lagged behind the peak in Chl-a, suggesting a consistent population of INPs associated with the collapse of phytoplankton blooms. The difference with the experiments conducted using the UNAM-MARAT is that no culture medium was added to induce blooms in our experiments. When comparing our results with the abovementioned studies (i.e., McCluskey et al. 2017; DeMott et al. 2016) before the addition of the culture medium (Day 0), we find that our INP concentrations are rather comparable with the values reported by both studies. However, the clear difference between the former studies and our results is that more efficient INPs were observed during the bloom conditions, as they nucleate ice at warmer temperatures (i.e., > -15°C), a situation not observed in our study. Another possible explanation for the observed differences between the present and former studies is that our samples likely contain a greater proportion of decomposed or dying material due to their transportation from the coast to the laboratory (Section 4.5).

As mentioned earlier, $n_s$ is a robust and quantitative metric for comparing the ice nucleating abilities of aerosol particles (Holden et al., 2021). Therefore, $n_s$ was calculated for each sample, as shown in Figure 10b. It was found that the highest and lowest $n_s$ values were derived from the BoA and BoSM samples, respectively. Although the BoSM sample had the highest particle concentration among the three analyzed samples (Figure 8), it exhibited the lowest $n_s$ values, indicating that the particles emitted from this water sample have fewer active sites for ice nucleation. DeMott et al. (2016) and McCluskey et al. (2017) report high $n_s$ values on the order of $1x10^{5}$ y $1x10^{6}$ $cm^{-2}$, respectively, which are consistent with the BoA values found in this study (Table S4).

### *4.4 Correlation of $T_{50}$ with Ion Concentration*

Spearman's correlation coefficients were calculated between the concentration of certain ions (since some could not be determined in specific particles sizes) and the median freezing temperature ($T_{50}$) to evaluate if the ice nucleation efficiency is associated with organic matter

(Figure S2). A better correlation was observed in the BoSM samples ($Na^+$ [$\rho = 0.94$, $p = 0.02$], $Cl^-$ [$\rho = 0.88$, $p = 0.03$], $Mg^{2+}$ [$\rho = 0.83$, $p = 0.06$], $Ca^{2+}$ [$\rho = 0.20$, $p = 0.71$], and $NO_3^-$ [$\rho = -0.08$, $p = 0.92$]) from April 9 and $Na^+$ [$\rho = 0.84$, $p = 0.04$], $Ca^{2+}$ [$\rho = 0.84$, $p = 0.04$], $Mg^{2+}$ [$\rho = 0.81$, $p = 0.07$], $NO_3^-$ [$\rho = -0.84$, $p = 0.04$], and $Cl^-$ [$\rho = -0.08$, $p = 0.87$] from April 25) than in the PoV sample ($Na^+$ [$\rho = 0.58$, $p = 0.24$], $NO_3^-$ [$\rho = 0.55$, $p = 0.27$], $Mg^{2+}$ [$\rho = 0.46$, $p = 0.37$], $Cl^-$ [$\rho = 0.46$, $p = 0.37$], and $Ca^{2+}$ [$\rho = -0.03$, $p = 0.98$]). While $Mg^{2+}$ showed a relatively high correlation in the BoSM samples, it did not reach the threshold for statistical significance ($p < 0.05$). This suggests that, while $Mg^{2+}$ may be present in SSA, its role in ice nucleation remains uncertain. Therefore, further research is needed to determine if $Mg^{2+}$ is a key driver in ice formation in marine environments. Moreover, the highest Spearman coefficients were found for the samples collected on the second day at BoSM, when the waters were turbid. Considering that the high concentrations of $Ca^{2+}$ and $Mg^{2+}$ ions are associated with continental particles that promote primary productivity in the coastal zone, their subsequent remineralization could mean that the BoSM sample collected on 04/09/22 was enriched in organic material, which explains the high ice nucleation efficiency observed in this sample.

### *4.5 Analysis of transport in the Manzanillo seawaters samples.*

Additional experiments were carried out with the BoSM samples to evaluate whether the transport of samples from the sampling site to our laboratory located in Mexico City affects the ice nucleating abilities of SSA generated in the UNAM-MARAT. Two water samples were taken in the BoSM. The 09/04/22 BoMS "fresh sample" results refer to experiments conducted on the second day after collection (experiments conducted in the field), and the 25/04/22 BoMS "aged sample" results refer to the experiments conducted 15 days after collection (experiments conducted in Mexico City). The sample was not preserved to maintain conditions similar to those applied to the BoA and PoV samples.

The particle concentration was higher in the aged sample for the sizes between 0.3 and 1.0 µm and those >10 µm. However, for particles between 1.0 and 10.0 µm, the highest concentrations were observed on the fresh samples as shown in Figure S3a.

Since it was observed that aging impacted the number of particles, the impact of aging on the ice nucleating abilities was also analyzed. The $n_s$ values were calculated for three temperatures (i.e., -20, -25, and -30°C). Figure S3b shows that the $n_s$ values were consistently higher in the aged sample. This could indicate that biological activity continued during the transport of the samples, which might explain the increase in $n_s$ values. However, ion concentrations did not change significantly between the fresh and aged samples. It is advisable to perform other chemical analyses to validate this hypothesis.

## 5 Conclusions

The UNAM-MARAT was specifically designed to simulate waves breaking to generate sea spray aerosol and to evaluate the ability of marine aerosol particles to act as INP. The ideal conditions established to work with the UNAM-MARAT were to use 40 L of seawater in the tank, employ a cascade with a slot length of 28.3 cm, and a plunging sheet intermittent cascade with an operating configuration of 2 s on and 10 s off to achieve particle concentrations exceeding 1000 $cm^{-3}$.

The UNAM-MARAT has proven to be an effective tool for evaluating and analyzing the physical and chemical properties of SSA from seawater samples collected at various locations. It offers a cost - effective alternative to expensive field campaigns, providing a controlled and reproducible method for simulating natural SSA generation. The results obtained from the UNAM-MARAT during its characterization are comparable to those obtained from other wave tanks, confirming its reliability and suitability for marine aerosol studies.

From the case study, we were able to successfully generate marine aerosol in the laboratory using seawater samples from various coastal areas of Mexico. The aerosol reached particle concentrations up to 2000 $cm^{-3}$ across a wide range of particles sizes, from 10 nm to 10 µm. Additionally, our results show that the Mexican oceanic waters contain INP with concentrations up to 130.7 $L^{-1}$. Among the three seawater samples analyzed, the BoA sample exhibited the highest ice nucleation abilities, based on the ice active site density values measured between -20 and -30°C. Furthermore, our findings reveal a direct relationship between particle size and composition. Larger particles (>1 µm) were found to be enriched in NaCl, whereas smaller particles showed an increased fraction of $Ca^{2+}$, $Mg^{2+}$, and $NO_3^-$ related to the presence and degradation of organic matter. However, it is important to note that the usage of a centrifugal pump could impact the marine microorganisms present in the natural seawater samples, potentially affecting their ice nucleating abilities.

The development of the UNAM-MARAT device and the comprehensive analysis of aerosol particles from different coastal regions contribute significantly to our understanding of the role of marine aerosol particles in mixed cloud formation and in the regional precipitation patterns. The newly built tank will serve as a valuable tool for future atmospheric and environmental studies.

***Data availability*.** Data are available upon request to the corresponding author.

***Author contributions*.** MFC, RC, and LAL designed and built the tank. MFC, GBR, and LAL designed the field campaign and the experiments. MFC, AO, GC, IM, and LAL carried out the field measurements and the collection of ambient samples. MFC, DRR, HAO, and TC performed the chemical analysis. MFC and LAL wrote the paper, with contributions from all coauthors.

***Competing interest.*** The authors declare that they have no conflict of interest.

***Acknowledgments.*** We thank Gabriel García, Manuel García, Omar López, and Victor García for their invaluable assistance in the construction and maintenance of the UNAM-MARAT. Also, we would like to thank Kenia Villela, Daniela Leal, María Isabel Saavedra, Dalia Aguilar, Eva Salinas, and Leticia Martínez for their assistance with the experiments related to the UNAM-MARAT. This study was financially supported by the PAPIIT IN111120 and IN106723 grants, the CONACYT fellowship for doctoral students, and the Marcos Moshinsky Foundation.

## References

Albrecht, B. A.: Aerosols, cloud microphysics, and fractional cloudiness, Science (80-. )., 245, 1227–1230, https://doi.org/10.1126/science.245.4923.1227, 1989.

Alpert, P. A., Aller, J. Y., and Knopf, D. A.: Ice nucleation from aqueous NaCl droplets with and without marine diatoms, Atmos. Chem. Phys., 11, 5539–5555, https://doi.org/10.5194/acp-11-5539-2011, 2011.

Anderson, D. M., Glibert, P. M., and Burkholder, J. M.: Harmful Algal Blooms and Eutrophication: Nutrient Sources, Composition, and Consequences, Estuaries, 25, 704–726, https://doi.org/10.1007/BF02804901, 2002.

Bates, T. S., Kapustin, V. N., Quinn, P. K., Covert, D. S., Coffman, D. J., Mari, C., Durkee, P. A., De Bruyn, W. J., and Saltzman, E. S.: Processes controlling the distribution of aerosol particles in the lower marine boundary layer during the first aerosol characterization experiment (ACE 1), J. Geophys. Res. Atmos., 103, 16369–16383, https://doi.org/10.1029/97JD03720, 1998.

Bates, T. S., Quinn, P. K., Frossard, A. A., Russell, L. M., Hakala, J., Petäjä, T., Kulmala, M., Covert, D. S., Cappa, C. D., Li, S. M., Hayden, K. L., Nuaaman, I., McLaren, R., Massoli, P., Canagaratna, M. R., Onasch, T. B., Sueper, D., Worsnop, D. R., and Keene, W. C.: Measurements of ocean derived aerosol off the coast of California, J. Geophys. Res. Atmos., 117, 1–13, https://doi.org/10.1029/2012JD017588, 2012.

Bigg, E. K.: Ice Nucleus Concentrations in Remote Areas, https://doi.org/10.1175/1520-0469(1973)030<1153:incira>2.0.co;2, 1973.

Bigg, E. K. and Leck, C.: The composition of fragments of bubbles bursting at the ocean surface, J. Geophys. Res. Atmos., 113, 1–7, https://doi.org/10.1029/2007JD009078, 2008.

Boucher, O., Randall, P. Artaxo, C., Bretherton, G., Feingold, P., Forster, V.-M., Kerminen, Y., Kondo, H., Liao, U., Lohmann, P., Rasch, S. K., Satheesh, S., Sherwood, B. S., and Zhang, X. .: Clouds and Aerosols. In: Climate Change 2013: The Physical Science Basis. Contribution of Working Group I to the Fifth Assessment Report of the Intergovernmental Panel on Climate Change, edited by: [Stocker, T. F., Qin, D., Plattner, G.-K., Tignor, M., Allen, S. K., Boschung, J., Nauels, A., Xia, Y., Bex, V., and Midgley, P. M. ., Cambridge, United Kingdom and New York, NY, USA. 571, 571–657 pp.,

https://doi.org/10.1017/CBO9781107415324.016, 2013.

Burrows, S. M., Hoose, C., Pöschl, U., and Lawrence, M. G.: Ice nuclei in marine air: Biogenic particles or dust?, Atmos. Chem. Phys., 13, 245–267, https://doi.org/10.5194/acp-13-245-2013, 2013.

Burrows, S. M., Ogunro, O., Frossard, A. A., Russell, L. M., Rasch, P. J., and Elliott, S. M.: A physically based framework for modeling the organic fractionation of sea spray aerosol from bubble film Langmuir equilibria, Atmos. Chem. Phys., 14, 13601–13629, https://doi.org/10.5194/acp-14-13601-2014, 2014.

Burrows, S. M., McCluskey, C. S., Cornwell, G., Steinke, I., Zhang, K., Zhao, B., Zawadowicz, M., Raman, A., Kulkarni, G., China, S., Zelenyuk, A., and DeMott, P. J.: Ice-Nucleating Particles That Impact Clouds and Climate: Observational and Modeling Research Needs, Rev. Geophys., 60, 1–45, https://doi.org/10.1029/2021RG000745, 2022.

Chakraborty, S., Bhattacharya, S., Feudel, U., and Chattopadhyay, J.: The role of avoidance by zooplankton for survival and dominance of toxic phytoplankton, Ecol. Complex., 11, 144–153, https://doi.org/10.1016/j.ecocom.2012.05.006, 2012.

Chow, J. C. and Watson, J. G.: Ion Chromatography in elemental analysis of airborne particles, Elemetal Anal. Airborne Part., 326, 1999.

Christiansen, S., Salter, M. E., Gorokhova, E., Nguyen, Q. T., and Bilde, M.: Sea Spray Aerosol Formation: Laboratory Results on the Role of Air Entrainment, Water Temperature, and Phytoplankton Biomass, Environ. Sci. Technol., 53, 13107–13116, https://doi.org/10.1021/acs.est.9b04078, 2019.

Cipriano, R. and Blanchard, C.: Bubble and Aerosol Spectra Produced by a Laboratory "Breaking Wave," J. Geophys. Res., 86, 8085–8092, 1981.

Collins, D. B., Zhao, D. F., Ruppel, M. J., Laskina, O., Grandquist, J. R., Modini, R. L., Stokes, M. D., Russell, L. M., Bertram, T. H., Grassian, V. H., Deane, G. B., and Prather, K. A.: Direct aerosol chemical composition measurements to evaluate the physicochemical differences between controlled sea spray aerosol generation schemes, Atmos. Meas. Tech., 7, 3667–3683, https://doi.org/10.5194/amt-7-3667-2014, 2014.

Córdoba, F., Ramírez-Romero, C., Cabrera, D., Raga, G. B., Miranda, J., Alvarez-Ospina, H., Rosas, D., Figueroa, B., Sung Kim, J., Yakobi-Hancock, J., Amador, T., Gutierrez, W., Garcia, M., Bertram, A. K., Baumgardner, D., and Ladino, L. A.: Measurement report : Ice nucleating abilities of biomass burning , African dust , and sea spray aerosol particles over the Yucatán Peninsula, Atmos. Chem. Phys., 21, 4453–4470, https://doi.org/10.5194/acp-21-4453-2021, 2021.

DeMott, P. J., Hill, T. C. J., McCluskey, C. S., Prather, K. A., Collins, D. B., Sullivan, R. C., Ruppel, M. J., Mason, R. H., Irish, V. E., Lee, T., Hwang, C. Y., Rhee, T. S., Snider, J. R., McMeeking, G. R., Dhaniyala, S., Lewis, E. R., Wentzell, J. J. B., Abbatt, J., Lee, C., Sultana, C. M., Ault, A. P., Axson, J. L., Martinez, M. D., Venero, I., Santos-Figueroa, G., Stokes, M. D., Deane, G. B., Mayol-Bracero, O. L., Grassian, V. H., Bertram, T. H., Bertram, A. K., Moffett, B. F., and Franc, G. D.: Sea spray aerosol as a unique source of ice nucleating

particles, Proc. Natl. Acad. Sci. U. S. A., 113, 5797–5803, https://doi.org/10.1073/pnas.1514034112, 2016a.

DeMott, P. J., Hill, T. C. J., McCluskey, C. S., Prather, K. A., Collins, D. B., Sullivan, R. C., Ruppel, M. J., Mason, R. H., Irish, V. E., Lee, T., Hwang, C. Y., Rhee, T. S., Snider, J. R., McMeeking, G. R., Dhaniyala, S., Lewis, E. R., Wentzell, J. J. B., Abbatt, J., Lee, C., Sultana, C. M., Ault, A. P., Axson, J. L., Diaz Martinez, M., Venero, I., Santos-Figueroa, G., Stokes, M. D., Deane, G. B., Mayol-Bracero, O. L., Grassian, V. H., Bertram, T. H., Bertram, A. K., Moffett, B. F., and Franc, G. D.: Sea spray aerosol as a unique source of ice nucleating particles, Proc. Natl. Acad. Sci., 113, 5797–5803, https://doi.org/10.1073/pnas.1514034112, 2016b.

Facchini, M. C., Rinaldi, M., Decesari, S., Carbone, C., Finessi, E., Mircea, M., Fuzzi, S., Ceburnis, D., Flanagan, R., Nilsson, E. D., de Leeuw, G., Martino, M., Woeltjen, J., and O'Dowd, C. D.: Primary submicron marine aerosol dominated by insoluble organic colloids and aggregates, Geophys. Res. Lett., 35, https://doi.org/10.1029/2008GL034210, 2008.

Fall, R. and Schnell, R. C.: Association of an ice-nucleating pseudomonad with cultures of the marine dinoflagellate, Heterocapsa niei., J. Mar. Res., 43, 257–265, https://doi.org/10.1357/002224085788437370, 1985.

Fuentes, E., Coe, H., Green, D., de Leeuw, G., and McFiggans, G.: Laboratory-generated primary marine aerosol via bubble-bursting and atomization, Atmos. Meas. Tech., 3, 141–162, https://doi.org/10.5194/amt-3-141-2010, 2010.

Harb, C. and Foroutan, H.: A Systematic Analysis of the Salinity Effect on Air Bubbles Evolution: Laboratory Experiments in a Breaking Wave Analog, J. Geophys. Res. Ocean., 124, 7355–7374, https://doi.org/10.1029/2019JC015337, 2019.

Hartery, S., MacInnis, J., and Chang, R. Y. W.: Effect of Sodium Dodecyl Benzene Sulfonate on the Production of Cloud Condensation Nuclei from Breaking Waves, ACS Earth Sp. Chem., 6, 2944–2954, https://doi.org/10.1021/acsearthspacechem.2c00230, 2022.

Hill, T. C. J., Demott, P. J., Tobo, Y., Fröhlich-Nowoisky, J., Moffett, B. F., Franc, G. D., and Kreidenweis, S. M.: Sources of organic ice nucleating particles in soils, Atmos. Chem. Phys., 16, 7195–7211, https://doi.org/10.5194/acp-16-7195-2016, 2016.

Holden, M. A., Campbell, J. M., Meldrum, F. C., Murray, B. J., and Christenson, H. K.: Active sites for ice nucleation differ depending on nucleation mode, Proc. Natl. Acad. Sci. U. S. A., 118, 1–9, https://doi.org/10.1073/pnas.2022859118, 2021.

Jacobson, M. Z.: Global direct radiative forcing due to multicomponent anthropogenic and natural aerosols, J. Geophys. Res. Atmos., 106, 1551–1568, https://doi.org/10.1029/2000jd900514, 2001.

Jelley, J. V.: Sea waves: their nature, behaviour, and practical importance, Endeavour, 13, 148–156, https://doi.org/10.1016/S0160-9327(89)80002-X, 1989.

Kennedy, F., Martin, A., Bowman, J. P., Wilson, R., and McMinn, A.: Dark metabolism: a molecular insight into how the Antarctic sea-ice diatom Fragilariopsis cylindrus survives

776 long-term darkness, New Phytol., 223, 675–691, https://doi.org/10.1111/nph.15843, 2019.

777 Knopf, D. A., Alpert, P. A., Wang, B., and Aller, J. Y.: Stimulation of ice nucleation by
778 marine diatoms, Nat. Geosci., 4, 88–90, https://doi.org/10.1038/ngeo1037, 2011.

779 Kuuppo, P., Autio, R., Kuosa, H., Setälä, O., and Tanskanen, S.: Nitrogen, silicate and
780 zooplankton control of the planktonic food-web in spring, Estuar. Coast. Shelf Sci., 46, 65–
781 75, https://doi.org/10.1006/ecss.1997.0258, 1998.

782 Ladino, L., Raga, G., Alvarez-Ospina, H., Andino-Enríquez, M., Rosas, I., Martínez, L.,
783 Salinas, E., Miranda, J., Ramírez-Díaz, Z., Figueroa, B., Chou, C., Bertram, A., Quintana,
784 E., Maldonado, L., Si, M., and Irish, V.: Ice-nucleating particles in a coastal tropical site,
785 Atmos. Chem. Phys., 19, 6147–6165, https://doi.org/10.5194/acp-19-6147-2019, 2019.

786 Ladino, L., Juaréz-Pérez, J., Ramírez-Díaz, Z., Miller, L. A., Herrera, J., Raga, G. B.,
787 Simpson, K. G., Cruz, G., Pereira, D. L., and Córdoba, F.: The UNAM-droplet freezing
788 assay: An evaluation of the ice nucleating capacity of the sea-surface microlayer and surface
789 mixed layer in tropical and subpolar waters, Atmosfera, 35, 127–141,
790 https://doi.org/10.20937/ATM.52938, 2022.

791 Lamarre, E. and Melville, W. K.: Air entrainment and dissipation in breaking waves.pdf,
792 Nature, 351, 469–472, https://doi.org/https://doi.org/ 10.1038/351469a0, 1991.

793 Lewis, E. R. and Schwartz, S. E.: Sea Salt Aerosol Production: Mechanisms, Methods,
794 Measurements and Models- A critical Review, American G., Washington, DC, 2004.

795 Mason, R. H., Si, M., Li, J., Chou, C., Dickie, R., Toom-Sauntry, D., Pöhlker, C., Yakobi-
796 Hancock, J. D., Ladino, L. A., Jones, K., Leaitch, W. R., Schiller, C. L., Abbatt, J. P. D.,
797 Huffman, J. A., and Bertram, A. K.: Ice nucleating particles at a coastal marine boundary
798 layer site: correlations with aerosol type and meteorological conditions, Atmos. Chem. Phys.,
799 15, 12547–12566, https://doi.org/10.5194/acp-15-12547-2015, 2015.

800 Mayer, K. J., Wang, X., Santander, M. V., Mitts, B. A., Sauer, J. S., Sultana, C. M., Cappa,
801 C. D., and Prather, K. A.: Secondary Marine Aerosol Plays a Dominant Role over Primary
802 Sea Spray Aerosol in Cloud Formation, ACS Cent. Sci., 6, 2259–2266,
803 https://doi.org/10.1021/acscentsci.0c00793, 2020.

804 McCluskey, C., Ovadnevaite, J., Rinaldi, M., Atkinson, J., Belosi, F., Ceburnis, D., Marullo,
805 S., Hill, T. C. J., Lohmann, U., Kanji, Z. A., O'Dowd, C., Kreidenweis, S. M., and DeMott,
806 P. J.: Marine and Terrestrial Organic Ice-Nucleating Particles in Pristine Marine to
807 Continentally Influenced Northeast Atlantic Air Masses, J. Geophys. Res. Atmos., 123,
808 6196–6212, https://doi.org/10.1029/2017JD028033, 2018.

809 McCluskey, C. S., Hill, T. C. J., Malfatti, F., Sultana, C. M., Lee, C., Santander, M. V., Beall,
810 C. M., Moore, K. A., Cornwell, G. C., Collins, D. B., Prather, K. A., Jayarathne, T., Stone,
811 E. A., Azam, F., Kreidenweis, S. M., and DeMott, P. J.: A dynamic link between ice
812 nucleating particles released in nascent sea spray aerosol and oceanic biological activity
813 during two mesocosm experiments, J. Atmos. Sci., 74, 151–166,
814 https://doi.org/10.1175/JAS-D-16-0087.1, 2017.

Melchum, A., Córdoba, F., Salinas, E., Martínez, L., Campos, G., Rosas, I., Garcia, E., Olivos, A., Raga, G. B., Pizano, B., Silva, M. M., and Ladino, L. A.: Maritime and continental microorganisms collected in Mexico: An investigation of their ice-nucleating abilities, Atmos. Res., 293, 106893, https://doi.org/10.1016/j.atmosres.2023.106893, 2023.

Prather, K. A., Bertram, T. H., Grassian, V. H., Deane, G. B., Stokes, M. D., DeMott, P. J., Aluwihare, L. I., Palenik, B. P., Azam, F., Seinfeld, J. H., Moffet, R. C., Molina, M. J., Cappa, C. D., Geiger, F. M., Roberts, G. C., Russell, L. M., Ault, A. P., Baltrusaitis, J., Collins, D. B., Corrigan, C. E., Cuadra-Rodriguez, L. A., Ebben, C. J., Forestieri, S. D., Guasco, T. L., Hersey, S. P., Kim, M. J., Lambert, W. F., Modini, R. L., Mui, W., Pedler, B. E., Ruppel, M. J., Ryder, O. S., Schoepp, N. G., Sullivan, R. C., and Zhao, D.: Bringing the ocean into the laboratory to probe the chemical complexity of sea spray aerosol, Proc. Natl. Acad. Sci. U. S. A., 110, 7550–7555, https://doi.org/10.1073/pnas.1300262110, 2013.

Quinn, P., Collins, D., Grassian, V., Prather, K., and Bates, T.: Chemistry and Related Properties of Freshly Emitted Sea Spray Aerosol, Chem. Rev., 115, 4383–4399, https://doi.org/10.1021/cr500713g, 2015.

Resch, F. and Afeti, G.: Submicron Film Drop Production by Bubbles in Sea Water, J. Geophys. Res., 97, 3679–3683, https://doi.org/https://doi.org/10.1029/91JC02961, 1992.

Rosinski, J., Haagenson, P. L., Nagamoto, C. T., and Parungo, F.: Nature of ice-forming nuclei in marine air masses, J. Aerosol Sci., 18, 291–309, https://doi.org/10.1016/0021-8502(87)90024-3, 1987.

Rosinski, J., Haagenson, P. L., Nagamoto, C. T., Quintana, B., Parungo, F., and Hoyt, S. D.: Ice-forming nuclei in air masses over the Gulf of Mexico, J. Aerosol Sci., 19, 539–551, https://doi.org/10.1016/0021-8502(88)90206-6, 1988.

Russell, L. M., Hawkins, L. N., Frossard, A. A., Quinn, P. K., and Bates, T. S.: Carbohydrate-like composition of submicron atmospheric particles and their production from ocean bubble bursting, Proc. Natl. Acad. Sci. U. S. A., 107, 6652–6657, https://doi.org/10.1073/pnas.0908905107, 2010.

Schnell, R. C.: Ice Nuclei in Seawater, Fog Water and Marine Air off the Coast of Nova Scotia: Summer 1975, J. Atmos. Sci., 34, 1299–1305, 1977.

Schnell, R. C. and Vali, G.: Freezing nuclei in marine waters, Tellus, 27, 321–323, https://doi.org/10.3402/tellusa.v27i3.9911, 1975.

Sellegri, K., Dowd, C. D. O., Yoon, Y. J., Jennings, S. G., and Leeuw, G. De: Surfactants and submicron sea spray generation, J. Geophys. Res., 111, D22215, https://doi.org/10.1029/2005JD006658, 2006.

Si, M., Irish, V. E., Mason, R. H., Vergara-Temprado, J., Hanna, S. J., Ladino, L. A., Yakobi-Hancock, J. D., Schiller, C. L., Wentzell, J. J. B., Abbatt, J. P. D., Carslaw, K. S., Murray, B. J., and Bertram, A. K.: Ice-nucleating ability of aerosol particles and possible sources at three coastal marine sites, Atmos. Chem. Phys., 18, 15669–15685, https://doi.org/10.5194/acp-18-15669-2018, 2018.

Stokes, M. D., Deane, G. B., Prather, K., Bertram, T. H., Ruppel, M. J., Ryder, O. S., Brady, J. M., and Zhao, D.: A Marine Aerosol Reference Tank system as a breaking wave analogue for the production of foam and sea-spray aerosols, Atmos. Meas. Tech., 6, 1085–1094, https://doi.org/10.5194/amt-6-1085-2013, 2013.

Thornton, D. C. O., Brooks, S. D., Wilbourn, E. K., Mirrielees, J., Alsante, A. N., Gold-bouchot, G., Whitesell, A., and Mcfadden, K.: Production of aerosol containing ice nucleating particles ( INPs ) by fast growing phytoplankton, Atmos. Chem. Phys. Discuss., [preprint], en revisión, https://doi.org/https://doi.org/10.5194/acp-2022-806, 2023a.

Thornton, D. C. O., Brooks, S. D., Wilbourn, E. K., Mirrielees, J., Alsante, A. N., Gold-Bouchot, G., Whitesell, A., and McFadden, K.: Production of ice-nucleating particles (INPs) by fast-growing phytoplankton, Atmos. Chem. Phys., 23, 12707–12729, https://doi.org/10.5194/acp-23-12707-2023, 2023b.

Trueblood, J. V., Wang, X., Or, V. W., Alves, M. R., Santander, M. V., Prather, K. A., and Grassian, V. H.: The Old and the New: Aging of Sea Spray Aerosol and Formation of Secondary Marine Aerosol through OH Oxidation Reactions, ACS Earth Sp. Chem., 3, 2307–2314, https://doi.org/10.1021/acsearthspacechem.9b00087, 2019.

Verdugo, P., Alldredge, A. L., Azam, F., Kirchman, D. L., Passow, U., and Santschi, P. H.: The oceanic gel phase: A bridge in the DOM-POM continuum, Mar. Chem., 92, 67–85, https://doi.org/10.1016/j.marchem.2004.06.017, 2004.

Vergara-Temprado, J., Murray, B. J., Wilson, T. W., O'Sullivan, D., Browse, J., Pringle, K. J., Ardon-Dryer, K., Bertram, A. K., Burrows, S. M., Ceburnis, D., Demott, P. J., Mason, R. H., O'Dowd, C. D., Rinaldi, M., and Carslaw, K. S.: Contribution of feldspar and marine organic aerosols to global ice nucleating particle concentrations, Atmos. Chem. Phys., 17, 3637–3658, https://doi.org/10.5194/acp-17-3637-2017, 2017.

Wang, X., Sultana, C. M., Trueblood, J., Hill, T. C. J., Malfatti, F., Lee, C., Laskina, O., Moore, K. A., Beall, C. M., McCluskey, C. S., Cornwell, G. C., Zhou, Y., Cox, J. L., Pendergraft, M. A., Santander, M. V., Bertram, T. H., Cappa, C. D., Azam, F., DeMott, P. J., Grassian, V. H., and Prather, K. A.: Microbial control of sea spray aerosol composition: A tale of two blooms, ACS Cent. Sci., 1, 124–131, https://doi.org/10.1021/acscentsci.5b00148, 2015.

Wang, X., Deane, G. B., Moore, K. A., Ryder, O. S., Stokes, M. D., Beall, C. M., Collins, D. B., Santander, M. V., Burrows, S. M., Sultana, C. M., and Prather, K. A.: The role of jet and film drops in controlling the mixing state of submicron sea spray aerosol particles, Proc. Natl. Acad. Sci. U. S. A., 114, 6978–6983, https://doi.org/10.1073/pnas.1702420114, 2017.

Wilson, T. W., Ladino, L. A., Alpert, P. A., Breckels, M. N., Brooks, I. M., Browse, J., Burrows, S. M., Carslaw, K. S., Huffman, J. A., Judd, C., Kilthau, W. P., Mason, R. H., McFiggans, G., Miller, L. A., Najera, J. J., Polishchuk, E., Rae, S., Schiller, C. L., Si, M., Temprado, J. V., Whale, T. F., Wong, J. P. S., Wurl, O., Yakobi-Hancock, J. D., Abbatt, J. P. D., Aller, J. Y., Bertram, A. K., Knopf, D. A., and Murray, B. J.: A marine biogenic source of atmospheric ice-nucleating particles, Nature, 525, 234–238, https://doi.org/10.1038/nature14986, 2015.

Wolf, M. J., Goodell, M., Dong, E., Dove, L. A., Zhang, C., Franco, L. J., Shen, C., Rutkowski, E. G., Narducci, D. N., Mullen, S., Babbin, A. R., and Cziczo, D. J.: A link between the ice nucleation activity and the biogeochemistry of seawater, Atmos. Chem. Phys., 20, 15341–15356, https://doi.org/10.5194/acp-20-15341-2020, 2020.

Wu, J. T. and Chou, T. L.: Silicate as the limiting nutrient for phytoplankton in a subtropical eutrophic estuary of Taiwan, Estuar. Coast. Shelf Sci., 58, 155–162, https://doi.org/10.1016/S0272-7714(03)00070-2, 2003.

Wurl, O., Werner, E., Landing, W. M., and Zappa, C. J.: Sea surface microlayer in a changing ocean - A perspective, Elem. Sci. Anthr., 5, 31, https://doi.org/10.1525/elementa.228, 2017.

Yakobi-Hancock, J. D., Ladino, L. A., and Abbatt, J. P. D.: Review of Recent Developments and Shortcomings in the Characterization of Potential Atmospheric Ice Nuclei: Focus on the Tropics, Rev. Ciencias, 17, 15–34, https://doi.org/10.25100/rc.v17i3.476, 2014.